Journal of
Synchrotron
Radiation

ISSN 0909-0495

Received 15 December 2004
Accepted 16 March 2005

High-energy phase-contrast X-ray imaging using a two-crystal X-ray interferometer

Akio Yoneyama,[a]* Tohoru Takeda,[b] Yoshinori Tsuchiya,[b] Jin Wu,[b] Thet-Thet Lwin,[b] Kazuyuki Hyodo[c] and Yasuharu Hirai[a]

[a]Advanced Research Laboratory, Hitachi Ltd, Hatoyama, Saitama 350-0395, Japan, [b]Graduate School of Comprehensive Human Sciences, University of Tsukuba, Tsukuba, Ibaraki 350-8575, Japan, and [c]Institute of Materials Science, High Energy Accelerator Research Organization, Tsukuba, Ibaraki 305-0801, Japan. E-mail: a-yoneya@rd.hitachi.co.jp

To broaden the scope of phase-contrast X-ray imaging in biomedical applications, the energy of X-rays in a large-area imaging system using a two-crystal X-ray interferometer has been increased from 17.7 keV to 35 keV. The use of higher-energy X-rays makes it possible to observe larger samples having greater variation in density within shorter measurement periods, at higher spatial resolution, and at lower X-ray doses. After optimizing the imaging system for 35 keV X-rays, a 25 mm × 30 mm interference pattern with 50% visibility was generated at the Photon Factory. The system's capabilities are demonstrated by this pattern and a high-quality three-dimensional image of a rat heart.

Keywords: phase contrast; X-ray imaging; two-crystal X-ray interferometer; high-energy X-rays.

1. Introduction

Phase-contrast X-ray imaging based on X-ray interferometry is a powerful tool for non-destructive biomedical imaging. Since the phase-shift cross section for a light element is about 1000 times bigger than the absorption cross section (Momose & Fukuda, 1995; Takeda *et al.*, 1995), this imaging technique provides a way of making fine observations of biological samples without the use of contrast agents and harmful X-ray doses. A monolithic triple Laue-case (LLL) X-ray interferometer (Bonse & Hart, 1965) has been applied to the radiographic observation of biological samples such as rat cerebella and metastatic liver tumors in humans (Momose & Fukuda, 1995; Takeda *et al.*, 1995).

Phase-contrast imaging has also been used in phase-contrast X-ray tomography (Momose, 1995). This technique was initially used with a monolithic interferometer, and was successfully applied to the non-destructive three-dimensional observation of small columnar samples of various biological soft tissues (Momose *et al.*, 1996; Beckmann *et al.*, 1997; Takeda *et al.*, 2000). However, this implementation is very limited in terms of the sizes of samples and observable ranges of variation in density. To broaden the technique's applicability, we need to extend these limits. As a step in this direction, the field of view has been extended by the adoption of a two-crystal X-ray interferometer (Fig. 1*a*) (Momose *et al.*, 1997; Yoneyama *et al.*, 1999, 2002; Yoneyama, Takeda, Tsuchiya, Wu, Lwin, Koizumi *et al.*, 2004). The latest version of this imaging system attained a 60 mm × 30 mm field of view. More recently, we have tried increasing the energy of the X-rays.

Higher-energy X-rays bring several advantages. Firstly, observable samples can be thicker, and details are more finely observed in shorter measurement periods and at lower X-ray doses. This is because the higher transmittance of the sample and the interferometer's crystal wafers for higher-energy X-rays leads to reduced absorption. Secondly, correct phase-maps (spatial distributions of the phase shifts caused by samples) can be obtained for samples having greater variation in density. Since higher-energy X-rays decrease the phase-shift cross sections, detected patterns have broader interference-fringe spacing, and this allows correct phase-unwrapping of phase shifts induced by materials with a greater range of density. Thirdly, spatial resolution is improved. This is due to the decreased Bragg angle, which corresponds to a narrower Borrmann fan within the crystal wafer.

Feasibility testing of even higher energy (35 and 51 keV) X-rays in phase-contrast imaging was performed with the aid of a monolithic LLL X-ray interferometer; the system successfully obtained an interference pattern with 50% visibility and achieved the two- and three-dimensional observation of large biological samples (Takeda, Wu, Tsuchiya, Yoneyama, Lwin, Hyodo & Itai, 2004; Takeda, Wu, Tsuchiya, Yoneyama, Lwin, Aiyoshi *et al.*, 2004). The results indicated the utility of high-energy X-rays for the observation of large samples. We now report on our optimization of the large-area imaging system (*i.e.* the system based on the two-crystal X-ray interferometer) for use with 35 keV X-rays, and give some results of performance testing in the form of an interference pattern and a three-dimensional image of a large biological sample.

2. Method and results

Increasing the energy of X-rays both raises the transmittance of samples and narrows the width of the field of view; that is, there is a trade-off between the thickness and width of observable samples. We selected 35 keV on the basis of this trade-off: at this level, the thickness, width and height of samples observable with our current

system are roughly the same. More precisely, the system parameters lead to a field of view 25 mm wide and 30 mm high. Transmittance through 30 mm of water is 77%, which is enough to generate an interference pattern with good visibility. In other words, we should be able to observe biological samples that would roughly fit within a 3 cm cube.

Using 35 keV rather than 17.8 keV X-rays required the following refinements to the imaging system. Firstly, the positioning tables carrying the crystal blocks of the interferometer were rearranged to maximize the field of view. Secondly, the upstream asymmetric crystal used to expand the incident beam was replaced by one with a lower degree of asymmetry (3.5°), which generates a 30 mm × 30 mm incident beam. Thirdly, the mechanical positioning accuracy of the active vibration isolator was improved from 5 μm to 0.2 μm by adopting a laser-displacement sensor; this allowed us to more accurately stabilize the beam's angle of incidence on the interferometer. Fourthly, the parameters of the feedback positioning system (Yoneyama, Takeda, Tsuchiya, Wu, Lwin & Hyodo, 2004), which compensates for the mechanical drift of the crystal blocks of the interferometer relative to each other, were tuned to suppress more accurately the phase fluctuations of the interference beams.

The performance of the refined imaging system was evaluated at the BL-14C1 beamline of the Photon Factory in Tsukuba, Japan. The vertically fan-shaped beam emitted from a vertical wiggler was monochromated by a Si(220) double-crystal monochromator and input to the imaging system. One of the generated interference patterns was detected by a CCD-based imaging sensor (36 mm × 36 mm field of view with 2048 pixels × 2048 pixels, each 18 μm × 18 μm) (Momose *et al.*, 2001), and the other was used by the feedback positioning system.

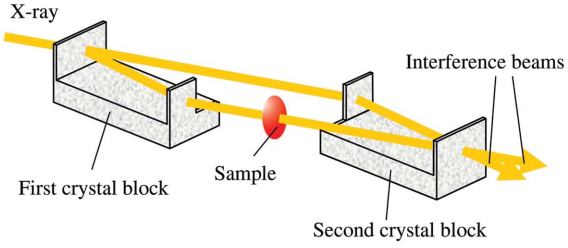

(*a*)

(*b*)

Figure 1
(*a*) Two-crystal X-ray interferometer and (*b*) a 25 mm × 30 mm interference pattern obtained with 35 keV X-rays. The fringe visibility was 50%, which is good enough to obtain phase-contrast images.

Fig. 1(*b*) shows an interference pattern obtained with a 3 s exposure. The pattern size was 25 mm wide and 30 mm high. The visibility was in the range from 40 to 60%, with an average of 50%, which is good enough for use in phase-contrast imaging. The average intensity was about 500 counts pixel^{-1} s^{-1}, which is double the intensity at 17.8 keV. This result showed that the use of high-energy X-rays enables the fine observation of large biomedical samples in only half of the measurement period required with the previous energy level. Since no object was placed in the beam path, the interference fringes observed in the figure were due to the lattice strain and/or deformation of the interferometer.

In the next step of performance testing, phase-contrast computed tomography (CT) was used in the non-destructive three-dimensional observation of biological samples. Fig. 2 shows one of the results: (*a*) a phase-contrast CT image of a rat heart fixed by formalin and cut away to reveal the internal structure, and (*b*) a magnified sectional image of the square in (*a*). The heart was about 16 mm in diameter and 15 mm high; the diameter is too great for clear observation at the previous energy level. To obtain the image, the sample was placed in a water-filled cell with a thickness of 20 mm, and then rotated in 0.72° steps (250 projections). The measurement procedure was the same as that described in a previous paper (Yoneyama, Takeda, Tsuchiya, Wu, Lwin & Hyodo, 2004). During this measurement, the feedback positioning system operated successfully, suppressing the phase fluctuation to within $\pi/15$. The high-density resolution of the imaging technique meant that the myocardium, papillary muscle and blood

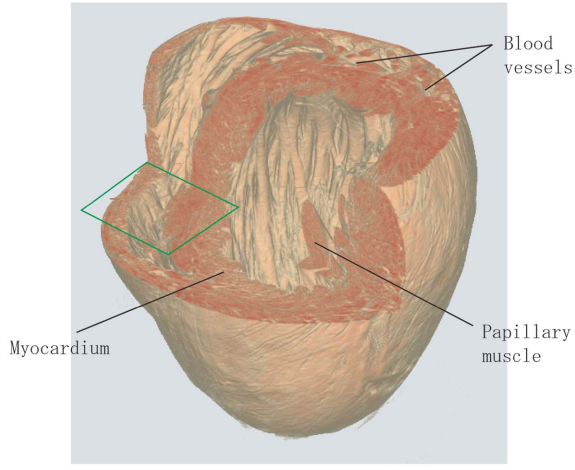

(*a*)

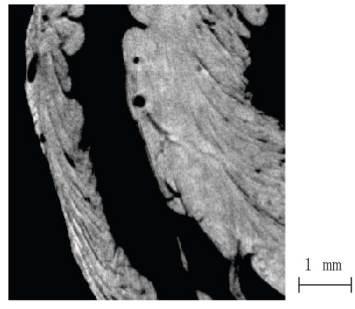

(*b*)

Figure 2
(*a*) A three-dimensional image of rat heart fixed by formalin and cut away to reveal the internal structure, and (*b*) a magnified sectional image of the square in (*a*). The organ was 16 mm in diameter and 15 mm high. The myocardium, papillary muscle and blood vessels are clearly visible and differentiated without the aid of a contrast agent.

vessels were clearly revealed and differentiated without the aid of contrast agents. Furthermore, blood vessels with a diameter of about 50 μm can be clearly seen in Fig. 2(*b*).

This experiment was approved by the University of Tsukuba's Medical Committee for the Use of Animals in Research and conforms to the guidelines of the American Physiological Society.

3. Conclusion

A 25 mm × 30 mm interference pattern was obtained by using 35 keV X-rays in a large-area phase-contrast X-ray imaging system based on a two-crystal X-ray interferometer. Clear three-dimensional observation of a rat heart was also performed. The results show how the use of higher-energy X-rays can broaden the scope of the imaging technique in biomedical application.

One of the other advantages of a two-crystal X-ray interferometer is the capability of suppressing a thermal disturbance caused by the sample's heat. In view of this advantage, *in vivo* three-dimensional observation with the same imaging system is our next goal. To date, feasibility testing and the observation of a cancer implanted in a nude mouse were successfully performed (Takeda, Yoneyama *et al.*, 2004). At the time of writing, we are proceeding with the next step: *in vivo* observation of the growth process of a cancer over a few days. To do this, we have designed a special sample holder and optimized the conditions and method of measurement for work with live mice. This method of observation will allow the *in vivo* evaluation of the effects of drugs in the near future.

This study was carried out under Proposal No. 2002S2-001 approved by the High Energy Accelerator Research Organization.

References

Beckmann, F., Bonse, U., Busch, F. & Gunnewig, O. (1997). *J. Comput. Assist. Tomogr.* **21**, 539–553.
Bonse, U. & Hart, M. (1965). *Appl. Phys. Lett.* **6**, 155–156.
Momose, A. (1995). *Nucl. Instrum. Methods*, A**352**, 622–628.
Momose, A. & Fukuda, J. (1995). *Med. Phys.* **22**, 375–380.
Momose, A., Takeda, T., Itai, Y. & Hirano, K. (1996). *Nature Med.* **2**, 473–475.
Momose, A., Takeda, T., Yoneyama, A., Koyama, I. & Itai, Y. (2001). *Nucl. Instrum. Methods*, A**467**, 917–920.
Momose, A., Yoneyama, A. & Hirano, K. (1997). *J. Synchrotron Rad.* **4**, 311–312.
Takeda, T., Momose, A., Hirano, K., Haraoka S., Watanabe, T. & Itai, Y. (2000). *Radiology*, **214**, 298–301.
Takeda, T., Momose, A., Itai, Y., Wu, J. & Hirano, K. (1995). *Acad. Radiol.* **2**, 799–803.
Takeda, T., Wu, J., Tsuchiya, Y., Yoneyama, A., Lwin, T. T., Aiyoshi, Y., Zeniya, T., Hyodo, K. & Ueno, E. (2004). *Jpn. J. Appl. Phys.* **43**, 5652–5656.
Takeda, T., Wu, J., Tsuchiya, Y., Yoneyama, A., Lwin, T. T., Hyodo, K. & Itai, Y. (2004). *AIP Conf. Proc.* **705**, 1328–1331.
Takeda, T., Yoneyama, A., Wu, J., Lwin, T. T., Tsuchiya, Y. & Hyodo, K. (2004). *Jpn. J. Appl. Phys.* **43**, L1144–1146.
Yoneyama, A., Momose, A., Koyama, I., Seya, E., Takeda, T., Itai, Y., Hirano, K. & Hyodo, K. (2002). *J. Synchrotron. Rad.* **9**, 277–281.
Yoneyama, A., Momose, A., Seya, E., Hirano, K., Takeda, T. & Itai, Y. (1999). *Rev. Sci. Instrum.* **70**, 4582–4586.
Yoneyama, A., Takeda, T., Tsuchiya, Y., Wu, J., Lwin, T. T. & Hyodo, K. (2004). *AIP Conf. Proc.* **705**, 1299–1302.
Yoneyama, A., Takeda, T., Tsuchiya, Y., Wu, J., Lwin, T. T., Koizumi, A., Hyodo, K. & Itai. Y. (2004). *Nucl. Instrum. Methods*, A**523**, 217–222.